Limnol. Oceanogr., 55(2), 2010, 950–964

Variable sediment oxygen uptake in response to dynamic forcing

Lee D. Bryant,[a,*] Claudia Lorrai,[b,c] Daniel F. McGinnis,[b,1] Andreas Brand,[b,2] Alfred Wüest,[b,c] and John C. Little[a]

[a] Civil and Environmental Engineering, Virginia Tech, Blacksburg, Virginia
[b] Eawag (Swiss Federal Institute of Aquatic Science and Technology), Surface Waters—Research and Management, Kastanienbaum, Switzerland
[c] Institute of Biogeochemistry and Pollutant Dynamics, ETH Zurich, Zurich, Switzerland

Abstract

Seiche-induced turbulence and the vertical distribution of dissolved oxygen above and within the sediment were analyzed to evaluate the sediment oxygen uptake rate (J_{O_2}), diffusive boundary layer thickness (δ_{DBL}), and sediment oxic zone depth (z_{max}) in situ. High temporal-resolution microprofiles across the sediment–water interface and current velocity data within the bottom boundary layer in a medium-sized mesotrophic lake were obtained during a 12-h field study. We resolved the dynamic forcing of a full 8-h seiche cycle and evaluated J_{O_2} from both sides of the sediment–water interface. Turbulence (characterized by the energy dissipation rate, ε), the vertical distribution of dissolved oxygen across the sediment–water interface (characterized by δ_{DBL} and z_{max}), J_{O_2}, and the sediment oxygen consumption rate (R_{O_2}) are all strongly correlated in our freshwater system. Seiche-induced turbulence shifted from relatively active ($\varepsilon = 1.2 \times 10^{-8}$ W kg^{-1}) to inactive ($\varepsilon = 7.8 \times 10^{-12}$ W kg^{-1}). In response to this dynamic forcing, δ_{DBL} increased from 1.0 mm to the point of becoming undefined, z_{max} decreased from 2.2 to 0.3 mm as oxygen was depleted from the sediment, and J_{O_2} decreased from 7.0 to 1.1 mmol m^{-2} d^{-1} over a time span of hours. J_{O_2} and oxygen consumption were found to be almost equivalent (within $\sim$ 5% and thus close to steady state), with R_{O_2} adjusting rapidly to changes in J_{O_2}. Our results reveal the transient nature of sediment oxygen uptake and the importance of accurately characterizing turbulence when estimating J_{O_2}.

Dissolved oxygen (O_2) is one of the most critical ecological parameters affecting natural aquatic systems with benthic diversity, ecosystem health, and overall water quality all negatively influenced by depleted O_2 levels (Wetzel 2001; Stachowitsch et al. 2007). The amount of O_2 taken up by the sediment largely governs O_2 depletion in stratified waters with organic-rich sediment (Bouldin 1968; Veenstra and Nolen 1991). Sediment O_2 uptake is a function of both physical limitations on O_2 transfer to the sediment and sediment O_2 consumption processes (Jørgensen and Boudreau 2001). Resolving the vertical distribution of O_2 at the sediment–water interface (SWI) allows for the quantification of the sediment O_2 uptake flux (J_{O_2}), which is a fundamental parameter for the characterization of O_2 dynamics in aquatic systems (Wetzel 2001). Consequently, considerable effort has been devoted to elucidating the water-side and sediment-side factors controlling sediment O_2 uptake in freshwater and marine systems (Bouldin 1968; Jørgensen and Revsbech 1985; Boudreau 2001).

Molecular diffusion typically becomes the controlling transport process for dissolved species (e.g., O_2) at approximately 1 mm above the SWI in nonadvective systems (e.g., cohesive freshwater and marine sediment; Jørgensen and Revsbech 1985; Røy et al. 2004). This millimeter-scale region immediately above the SWI is referred to as the diffusive boundary layer (DBL; Jørgensen and Revsbech 1985). Diffusion through the DBL is often the rate-limiting step restricting the supply of O_2 to the sediment in systems (e.g., lakes) where steep gradients occur at the SWI (Jørgensen and Revsbech 1985; Wüest and Lorke 2003). O_2 transport to the SWI is driven by the concentration gradient in the DBL and is therefore a function of the thickness of the DBL (δ_{DBL}), which is controlled by turbulent mixing in the bottom boundary layer (BBL), and O_2 concentrations within the bulk BBL (C_{bulk}) and at the SWI (C_{SWI}), as depicted in Fig. 1. Upon reaching the sediment, O_2 is used for various biogeochemical processes (e.g., benthic organic matter mineralization and oxidation of reduced compounds) within the sediment oxic zone (quantified by depth z_{max}; Fig. 1). A balance between the rate at which O_2 is supplied to the sediment, quantified by flux J_{O_2} (mmol m^{-2} d^{-1}), and the rate at which O_2 is consumed within the sediment, quantified by the O_2 consumption rate (R_{O_2}), which may be defined volumetrically ($R_{O_2 v}$; mmol m^{-3} d^{-1}) or areally ($R_{O_2 a}$; mmol m^{-2} d^{-1}), establishes the extent of the sediment oxic zone (Jørgensen and Boudreau 2001; Higashino et al. 2004). It is important to note that R_{O_2} describes the use of available O_2 supplied to the sediment rather than the potential sediment O_2 demand (PSOD), which is often evaluated as a constant volumetric O_2 consumption rate. PSOD is a function of available electron acceptors in the sediment. While $R_{O_2 v}$ may approach PSOD in systems where $R_{O_2 v}$ controls O_2 diffusion at the SWI (e.g., marine sediment), PSOD would be much greater than $R_{O_2 v}$ in highly organic, transport-limited systems (e.g., lake sedi-

* Corresponding author: lebryan1@vt.edu

Present address:
[1] IFM-GEOMAR, Leibniz Institute of Marine Sciences, RD2 Marine Biogeochemistry, Kiel, Germany
[2] Civil and Environmental Engineering, University of California, Berkeley

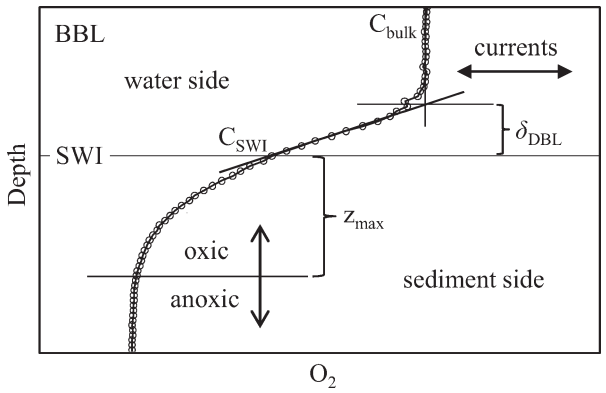

Fig. 1. The key components of a dissolved oxygen (O_2) profile are defined, illustrating the relationship between seiching, turbulent mixing, and the vertical distribution of O_2 on both sides of the sediment–water interface (SWI; modified from Jørgensen and Revsbech 1985). Water-side components include the bottom boundary layer (BBL), the diffusive boundary layer (of thickness δ_{DBL}), and O_2 concentrations in the BBL (C_{bulk}) and at the SWI (C_{SWI}). On the sediment side, z_{max} is the depth of the sediment oxic zone.

ment; Wüest and Lorke 2003). Furthermore, while $R_{O_2 v}$ may be strongly influenced by J_{O_2}, PSOD is a relatively inherent property unaffected by short-term variations in O_2 availability.

Turbulence in the BBL (e.g., due to internal currents forced by wind or tide) has a direct effect on O_2 transport to the sediment and thus also influences O_2 consumption processes within the sediment. Significant insight has been gained from theoretical studies on how turbulence-induced variations in δ_{DBL} affect O_2 uptake (Higashino et al. 2004, 2008), the relative contributions of O_2-consuming processes (Glud et al. 2007; Brand et al. 2009), and sediment microbial activity (Gantzer and Stefan 2003; Higashino and Stefan 2005). Rapid changes in δ_{DBL} in response to dynamic forcing have been observed both in the laboratory (Mackenthun and Stefan 1998; Røy et al. 2004; O'Connor and Hondzo 2008) and in situ (Gundersen and Jørgensen 1990; Lorke et al. 2003). Glud et al. (2009) document that the vertical distribution of O_2 at the SWI of marine sediment can vary temporally (on the order of minutes to hours) by a factor > 3, which is within the range of seasonal variability for many aquatic systems. Results of these studies highlight the importance of using multiple measurements to resolve average conditions at the SWI. However, isolated measurements evaluating J_{O_2} under conditions assumed constant are sometimes extrapolated to characterize an aquatic system, thereby ignoring the influence of intermittent hydrodynamic processes (Veenstra and Nolen 1991; Beutel 2003).

Despite the established relationship between turbulence and the vertical O_2 distribution near the SWI, relatively few studies have incorporated simultaneous measurements of in situ current velocity and δ_{DBL} into the assessment of J_{O_2}. Previous work has focused predominantly on marine systems (Gundersen and Jørgensen 1990; Glud et al. 2007). Several freshwater experiments were performed to resolve turbulent O_2 transport within the BBL (Brand et al. 2008) and the effect of BBL dynamics on δ_{DBL} (Lorke et al. 2003); however, these studies primarily characterized turbulence. To our knowledge, no in situ work has been done that focuses on how J_{O_2}, δ_{DBL}, and the sediment oxic zone vary in response to rapid changes in velocity and direction of basin-scale (i.e., seiche) currents. Additionally, while sediment O_2 uptake may be influenced by both hydrodynamics and consumption processes within the sediment (Fig. 1), J_{O_2} is almost always interpreted exclusively from either a water- or sediment-side perspective (Higashino et al. 2004). We performed an in situ study that evaluated data from the water and sediment side of the SWI to determine how seiche-induced turbulence affects δ_{DBL}, the sediment oxic zone, and corresponding J_{O_2} and R_{O_2} on a rapid (subhourly) timescale. This research is therefore unique in that it assesses the transient nature of sediment O_2 uptake by investigating the effect of seiche-induced dynamic forcing on the vertical O_2 distribution under natural, in situ conditions from both sides of the SWI.

Methods

Study site and in situ instrumentation—We performed a 12-h field campaign (21:00 h on 27 August to 09:00 h on 28 August 2007) to obtain high-resolution SWI profile data (O_2 and temperature) and velocity data in Lake Alpnach, Switzerland. Lake Alpnach has a simple elliptical shape, a well-established deep current structure, and mesotrophic production (Wüest et al. 2000). The lake is characterized by a relatively high J_{O_2} (ranging annually from $\sim$ 10 to $\sim$ 20 mmol m^{-2} d^{-1}) and a shallow sediment oxic zone (< 3 mm) that establish steep O_2 gradients at the SWI (Müller et al. 2002; Lorke et al. 2003). Alpine mountain ridges direct thermal winds over the lake causing basin-scale movements of the waterbody. Two seiche modes are typically observed in summer: a first horizontal–first vertical mode with a period of 8 to 12 h and a first horizontal–second vertical mode with a period of $\sim$ 24 h (Münnich et al. 1992; Lorke et al. 2003). The dynamic O_2 conditions at the SWI and daily wind forcing make Lake Alpnach an ideal location for this study.

During the campaign, an instrumentation array was deployed on the southwestern slope of Lake Alpnach (46°57′21″N, 8°17′53″E) at a depth of 22 m. Velocity data were collected continuously at a single point using an acoustic Doppler velocimeter (ADV; Vector, Nortek) and as vertical profiles using an acoustic Doppler profiler (ADP; Aquadopp, Nortek). Thermistors (TR-1060, RBR Ltd.) were placed on the ADP tripod to resolve the temperature structure. A microprofiler (MP4, Unisense A/S) was used to measure high-resolution O_2 and temperature profiles across the SWI. A conductivity–temperature–depth (CTD; SBE-19, Seabird Electronics) profiler, which also measured O_2, was used to profile the water column near the experiment site every 2 h for background information on O_2 and density stratification. Detailed information about the primary components of the experimental setup is provided below. Frequently used acronyms and notations are defined in Table 1.

ADV velocity measurements—An ADV was used to continuously measure three-dimensional current time series

Table 1. Acronyms and notations with corresponding units used for this study.

ADP	Acoustic Doppler Aquadopp profiler; used to obtain velocity profile data
ADV	Acoustic Doppler velocimeter; used to obtain local (pointwise), high-frequency velocity data
BBL	Bottom boundary layer
D	Molecular O_2 diffusion coefficient ($m^2\ d^{-1}$)
DBL	Diffusive boundary layer
C_{bulk}	Concentration of O_2 in bulk BBL ($\mu mol\ L^{-1}$)
C_{SWI}	Concentration of O_2 at SWI ($\mu mol\ L^{-1}$)
$\partial C/\partial t_v$	Volumetric change in O_2 concentration over time ($mmol\ m^{-3}\ d^{-1}$)
$\partial C/\partial t_a$	Areal change in O_2 concentration over time ($mmol\ m^{-2}\ d^{-1}$)
$\partial C/\partial z$	O_2 concentration gradient ($mmol\ m^{-4}$)
J_{O_2}	SWI flux of O_2 into the sediment ($mmol\ m^{-2}\ d^{-1}$)
M_{O_2}	Vertically integrated mass of O_2 in sediment ($\mu mol\ m^{-2}$)
O_2	Dissolved oxygen ($\mu mol\ L^{-1}$)
PSOD	Potential sediment O_2 demand ($mmol\ m^{-3}\ d^{-1}$)
R_{O_2}	O_2 consumption rate in sediment, defined volumetrically (R_{O_2v}) or areally (R_{O_2a})
R_{O_2a}	Areal O_2 consumption rate in sediment ($mmol\ m^{-2}\ d^{-1}$) where R_{O_2a} is the vertical integral of volumetric R_{O_2v} (Eq. 2)
R_{O_2v}	Volumetric O_2 consumption rate in sediment ($mmol\ m^{-3}\ d^{-1}$)
SWI	Sediment–water interface
u_*	Friction velocity ($cm\ s^{-1}$)
z	Distance above or below SWI (mm)
z_{max}	Depth of sediment oxic zone (mm)
δ_{DBL}	DBL thickness (mm)
ε	Dissipation rate of turbulent kinetic energy ($W\ kg^{-1}$)
φ	Porosity (void volume per total sediment volume; dimensionless)
σ	Standard deviation (units correspond to parameter of interest)

at 32 Hz, positioned via tripod at 10 cm above the SWI. Accuracy of the velocity measurements is 0.5% of measured value $\pm 0.1\ cm\ s^{-1}$. ADV velocity data were used to analyze the current structure and to estimate energy dissipation rate and friction velocity at 10 cm above the SWI.

ADP velocity measurements—A 2-MHz ADP equipped with three acoustic beams slanted at 25° was used to measure BBL current profiles. Accuracy of the velocity measurements is 1% of measured value $\pm 0.5\ cm\ s^{-1}$. The ADP was positioned (via tripod) downward looking and measured profiles from 1.60 m to 0 m above the sediment, with 32 measurement cells (5-cm bin size). Samples were obtained in burst mode with 1024 samples per ensemble at a rate of 8 Hz. ADP velocity data were used to estimate bottom drag coefficients at 1 m above the SWI as an independent verification of ADV velocity data.

O_2 *and temperature logger measurements*—BBL temperature (i.e., density) structure was continuously measured using a string of 20 thermistors positioned every 25 cm on the leg of the ADP tripod, from 0 m to 4.75 m above the sediment. Measurements were obtained using TR-1060 thermistors, which have a response time of < 3 s, accuracy of $\pm 2 \times 10^{-3}$ °C, resolution of $< 5 \times 10^{-5}$ °C, and drift of $< 2 \times 10^{-3}$ °C yr^{-1}. A logger measuring both temperature and O_2 (TDO-2050, RBR Ltd.) was mounted on the microprofiler at 8 cm above the sediment. In addition to TR-1060 temperature specifications, the TDO-2050 has a measurement range of 0% to 150% O_2 saturation, with an accuracy of ±1%. TDO-2050 O_2 data were calibrated via Winkler titration of BBL water sampled at the same depth using a Niskin bottle. The calibrated TDO time series and a zero reading from anoxic sediment were then used for calibration of microprofiler O_2 measurements.

Microsensor O_2 *and temperature measurements across SWI*—An in situ autonomous microprofiler equipped with microsensors (one Clark-type O_2 sensor and one thermocoupled temperature sensor, Unisense A/S) was used for microprofiling across the SWI. The sensors have tip diameters of 100 μm, which allow for fast response time (90% in < 8 s), negligible stirring sensitivity, and $\sim$ 100-μm spatial resolution. Vertical alignment of the microsensors was established by lowering the group of microsensors toward quiescent water and adjusting sensors until all tips touched the water surface simultaneously. Profiles were obtained every $\sim$ 50 min and were acquired as follows: 10-mm resolution from 10 cm to 1 cm above the SWI, 1-mm resolution from 1 cm to 0.5 cm above the SWI, 0.1-mm resolution from 0.5 cm above to 0.5 cm below the SWI. Following a brief pause to establish equilibrium, ten data points were collected at each depth at a rate of 1 Hz (inspection of measurement set showed no trend in variation, thus confirming data aliasing did not occur).

We measured 14 O_2 profiles during the experiment. The O_2 profile number (1–14) corresponds to the time each profile was obtained and is used as a reference for comparison with other parameters (e.g., turbulence). In the absence of a video camera, the location of the SWI was determined by both visual interpretation of each profile (based on identifying linear DBL regions and kinks in the profiles due to porosity differences between the sediment and the water column; Røy et al. 2004) and using standard deviations of O_2 profile data (variation should decrease approaching the SWI due to reduced fluctuations in turbulence; Müller et al. 2002; Brand et al. 2007). Estimates of the SWI using O_2 standard deviations were comparable to estimates based on visual interpretation, though consistently $\sim$ 1 mm deeper. Correspondingly, previous work has shown the variance method to systematically overestimate δ_{DBL} due to concentration fluctuations protruding into the sediment (Røy et al. 2004). The SWI location predicted by both methods did remain relatively constant across our profile series, however. Hence, even if the estimated SWI location was slightly erroneous, this would not affect comparison among profiles.

O_2 *uptake and DBL analyses*—O_2 uptake is frequently evaluated for cohesive sediment using a water-side approach based on Fick's first law of diffusion (Rasmussen

and Jørgensen 1992)

$$J_{O_2} = \varphi D \frac{\partial C}{\partial z} = \varphi D \frac{C_{bulk} - C_{SWI}}{\delta_{DBL}} \left[\text{mmol m}^{-2}\ \text{d}^{-1}\right] \quad (1)$$

where D is the molecular diffusion coefficient for O_2 in water ($m^2\ d^{-1}$), φ is porosity (m^3 voids m^{-3} total volume; taken as unity in the water column), and $\partial C/\partial z$ is the linear O_2 concentration gradient in the DBL immediately above the SWI (i.e., the change in the O_2 concentration, C, over distance z; mmol m^{-4}).

While this is one of the most direct approaches for evaluating J_{O_2}, there are several problems associated with quantifying δ_{DBL}. The short residence time of O_2 near the SWI and rapid variations in δ_{DBL} due to BBL turbulence make it difficult to accurately characterize the DBL with microsensor measurements (Røy et al. 2004; O'Connor and Hondzo 2008). Furthermore, the transition from the linear DBL to the bulk BBL region is often indistinct (Wüest and Lorke 2003). To address this issue, Jørgensen and Revsbech (1985) established an ''effective'' DBL, obtained by extrapolating $\partial C/\partial z$ at the SWI to the point where O_2 levels reach the average concentration of the BBL (C_{bulk}; Fig. 1) as defined by the second part of Eq. 1 (on the right-hand side). It has been shown, however, that δ_{DBL} is often overestimated by the effective DBL (Hondzo et al. 2005; O'Connor and Hondzo 2008). Additionally, microsensors have been found to alter the structure of the DBL by ~ 25–45%, possibly due to increased flow around the microsensor shaft compressing the DBL below the sensor tip (Glud et al. 1994; Glud 2008). A decreased δ_{DBL} caused by microsensor compression would obviously result in an overestimation of J_{O_2}. Considering the variability of the DBL and subsequent difficulties in characterizing δ_{DBL}, it may be more appropriate to regard δ_{DBL} as a conceptual parameter rather than as a physical quantity.

Although problems with quantifying δ_{DBL} are avoided when using sediment-side methods, these methods are often more intensive due to relatively complex sediment processes. In addition to accounting for φ effects (Eq. 1), changes in O_2 consumption and storage in the sediment must also be accurately quantified. The balance between the amount of O_2 taken up by the sediment (characterized by J_{O_2}) and the amount consumed within the sediment (characterized by R_{O_2}) is shown by

$$J_{O_2} = \int_0^{z_{max}} R_{O_2 v}\, dz + \int_0^{z_{max}} \frac{\partial C}{\partial t_v}\, dz \left[\text{mmol m}^{-2}\ \text{d}^{-1}\right] \quad (2)$$

where volumetric $R_{O_2 v}$ (mmol $m^{-3}\ d^{-1}$) and the change in O_2 concentration over time ($\partial C/\partial t_v$; mmol $m^{-3}\ d^{-1}$) are integrated over the sediment profile to z_{max} (designated in this study as the depth where $O_2 < 3$ μmol L^{-1}). The first term on the right-hand side of Eq. 2 represents the amount of O_2 consumed per unit of time, while the second term represents the temporal change of the O_2 content in the sediment (Higashino et al. 2004). Depth-integrated values from Eq. 2 are defined by areal $R_{O_2 a}$ and $\partial C/\partial t_a$, respectively (mmol $m^{-2}\ d^{-1}$; Table 1), for each profile to allow for direct comparison with J_{O_2}. Equation 2 shows that J_{O_2} and $R_{O_2 a}$ are equal at steady state, whereas O_2 accumulation or depletion ($\partial C/\partial t_a$) occurs during transient conditions.

To comprehensively assess how dynamic forcing affects sediment O_2 uptake, we analyzed J_{O_2} and δ_{DBL} for each O_2 microsensor profile with five different methods that incorporated data from both the water side (direct and u_* methods) and sediment side (curvefit, zonefit, and model methods) of the SWI. These five methods were selected to evaluate J_{O_2} using O_2 microsensor and velocity data. Problems with specific measurement techniques (e.g., measuring δ_{DBL}) or analytical methods should be minimized by the use of a combination of methods based on water-side velocities and water- and sediment-side microsensor data. A more detailed comparison of the methods used to estimate sediment O_2 uptake will be presented in a companion paper (L. Bryant unpubl. data).

For the direct method, $\partial C/\partial z$ was obtained directly from the DBL region of O_2 microsensor profiles and then incorporated into Eq. 1 to evaluate δ_{DBL} and J_{O_2} (Jørgensen and Revsbech 1985). For the u_* method (Hondzo et al. 2005), dimensionless power law scaling was applied to friction velocity (u_*) data derived from ADV velocity series to universally scale the vertical O_2 distribution in the BBL for δ_{DBL}, which was then used to solve for J_{O_2} via Eq. 1.

O_2 profile data from the sediment side were evaluated by fitting a polynomial equation $C(z)$ to the porewater region of each O_2 profile, focusing on the region immediately below the SWI (curvefit method). The derivative of $C(z)$ was then incorporated into Eq. 1 to solve for J_{O_2} and δ_{DBL} (Glud 2008). Third-order $C(z)$ polynomial equations were found to best fit the series of profile data, with the exception of profile 6, which required a fourth-order polynomial.

Porewater data were also evaluated using the numerical model PROFILE (Berg et al. 1998), which analyzes data based on a numerical analysis that defines multiple zones of constant consumption to best describe each O_2 profile (zonefit method). Integrating depth-specific $R_{O_2 v}$ (evaluated at 0.1-mm increments) over the depth of the sediment oxic zone yields the overall areal $R_{O_2 a}$ per profile. $R_{O_2 a}$ can then be used to calculate J_{O_2} via Eq. 2. Model parameters used include $D = 1.97 \times 10^{-9}$ $m^2\ s^{-1}$ at 20°C (corrected for temperature using the Stokes–Einstein relationship; Li and Gregory 1974; Agrega and Lee 2005), with irrigation and bioturbation effects assumed negligible and boundary conditions (evaluated at the bottom of each profile) of $J_{O_2} = 0$ mmol $m^{-2}\ d^{-1}$ and $C = 0$ μmol L^{-1}.

We further analyzed sediment porewater data with the sediment module of the aquatic system simulation software AQUASIM (Reichert 1994), which was used to predict the δ_{DBL} required to model O_2 porewater profiles via a simple Monod model for O_2 consumption (model method). Model parameters and setup details for the AQUASIM model used in this study are defined by Brand et al. (2009). We were able to accurately model our series of sediment O_2 profiles in AQUASIM with a single set of Monod parameters (maximum oxidation rate (μ) = 5920 mmol $m^{-3}\ d^{-1}$ and half-saturation constant (K_{O_2}) = 19.1 μmol L^{-1}) and C_{SWI} as the only variable. We then incorporated these Monod parameters into a second model (see Eq. 6 in Brand et al. 2009) in which C_{bulk} was designated as the

upper boundary condition and δ_{DBL} was used as the sole fitting parameter to reproduce our sediment O_2 profiles.

Sediment cores from our experiment site were analyzed for φ (porewater volume per total volume) following Dalsgaard et al. (2000) to characterize diffusive transport in the sediment, and φ values of 0.97 and 0.91 in the upper 5 mm were obtained. Using these φ results as a point of reference and J_{O_2} values from an independent set of profiles (obtained ~ 1 m from our experiment site, measured prior to the series of 14 assessed in the primary study) as goals, φ was also estimated on a millimeter scale with PROFILE (which uses φ as an input parameter) via a trial-and-error approach. Similar porosities (0.95 in the upper 1 mm of sediment and 0.90 below) were obtained, and these φ values were used in Eq. 1 and/or as model parameters.

The transience of our system and sediment O_2 consumption as a function of O_2 availability were evaluated using Eq. 2. Proximity to steady state was determined by calculating $\partial C/\partial t_a$ for each profile by comparing the preceding and following profiles, evaluating $\partial C/\partial t_v$ at each depth, and integrating over z_{max}. Because the direct, u_*, curvefit, and model methods estimate J_{O_2} directly, results from these methods were used to evaluate O_2 consumption (as characterized by R_{O_2a}) via Eq. 2 as a function of $\partial C/\partial t_a$. The zonefit method predicts depth-specific O_2 consumption directly, and hence Eq. 2 was used to estimate J_{O_2} from R_{O_2a} values based on PROFILE results.

Using results of the five methods, mean values of J_{O_2}, R_{O_2a}, and δ_{DBL} were calculated for each profile. These parameters were statistically analyzed based on a normal distribution. Standard deviations (σ) were calculated for J_{O_2} and δ_{DBL} data (σ calculations for R_{O_2a} were unnecessary since J_{O_2} and R_{O_2a} are directly correlated via Eq. 2). Estimates obtained from the five methods were comparable, as shown below.

Inertial dissipation analyses—The dissipation rate of turbulent kinetic energy, ε (W kg^{-1}), was estimated using the inertial dissipation method (Grant et al. 1962). The analysis is based on the inertial subrange where the spectrum is expressed in the wave number (k) domain

$$E(k) = \alpha \varepsilon^{2/3} k^{-5/3} \left[\mathrm{m^3\ s^{-2}}\right] \quad (3)$$

where velocity fluctuation follows a $k^{-5/3}$ slope for eddy sizes of typically decimeters to meters (Fig. 2a). We used $\alpha = 1.56$ for the experimentally estimated, three-dimensional Kolmogorov constant (Wyngaard and Coté 1971). With the ADV, we measured horizontal (longitudinal and lateral) and vertical velocity fluctuations 10 cm above the sediment. Dissipation rates can be obtained from the longitudinal component of the one-dimensional spectrum expressed in the wave number (k_1) domain

$$\varphi_{11}(k_1) = \alpha_1 \varepsilon^{2/3} {k_1}^{-5/3} \left[\mathrm{m^3\ s^{-2}}\right] \quad (4)$$

and the two transversal components of the power spectrum

$$\varphi_{22}(k_1) = \varphi_{33}(k_1) = \alpha_2 \varepsilon^{2/3} {k_1}^{-5/3} \left[\mathrm{m^3\ s^{-2}}\right] \quad (5)$$

where $\alpha_1 = (18/55)\ \alpha$ and $\alpha_2 = (4/3)\ \alpha_1$. Rather than fitting the $-5/3$ slope to the inertial subrange, the respective power spectrum (Eqs. 4 and 5) is multiplied by $k^{5/3}$. This procedure transforms the spectrum so that it is only dependent on ε as $E(k) \times k^{5/3}$ becomes constant (Fig. 2a). Dissipation (ε) is then calculated by taking the average of the inertial subrange. All three velocity fluctuation records were used to quantify the value of ε (longitudinal, transversal planar, and transversal vertical; Eqs. 4 and 5) over a time span of approximately 50 min (Fig. 2b), which corresponds to the measurement period of each O_2 profile.

To account for the intermittency of turbulence, ε is averaged by assuming a lognormal distribution (Baker and Gibson 1987). The most likely average of the three ε values ($\bar{\varepsilon}$) is

$$\bar{\varepsilon} = \exp\left(\overline{\ln(\varepsilon)} + \frac{\sigma^2_{\ln(\varepsilon)}}{2}\right) \left[\mathrm{W\ kg^{-1}}\right] \quad (6)$$

where $\overline{\ln(\varepsilon)}$ is the average of the ln value of ε and $\sigma_{\ln(\varepsilon)}$ is the standard deviation, or intermittency, of the ln (ε) values (Table 2).

Friction velocity analyses—Friction velocities (u_*) were calculated at a height (h) of 10 cm above the sediment from the estimated ε values using the law-of-the-wall assumption

$$u_* = \sqrt[3]{\varepsilon \kappa h} \left[\mathrm{m\ s^{-1}}\right] \quad (7)$$

where κ (the von Karman constant) is 0.41. The resulting u_* values (Table 2) quantify the frictional stress of BBL currents on the sediment and, thus, like ε, describe the level of turbulence in the BBL.

Results

Seiche dynamics—We acquired data for 12 h and captured a full 8-h seiche cycle. During the campaign, bottom currents moved initially from the southwest toward the northeast, reached the current reversal point, and then reversed direction toward the southwest, similar to the motion of a pendulum (as depicted in Fig. 3a, where the schematics show the waterbody moving back and forth relative to our experiment site). Corresponding changes in current velocity are shown in Fig. 3b. During the observed seiche cycle, water from higher elevations in the BBL moved down the southwestern slope with increasing velocity toward the northeast. Current velocity reached a maximum of 2.3 cm s^{-1} (at 23:50 h) during this period. At the current reversal point (~ 04:00 h), velocities in the BBL reached a minimum value of 0.6 cm s^{-1}. When the water mass then shifted back toward the southwest, water from the central region of the BBL moved toward the southwestern slope and velocities increased to levels observed prior to current reversal, reaching a maximum value of 2.3 cm s^{-1} (at 07:44 h).

Lorke et al. (2002) demonstrated that law-of-the-wall theory (used to estimate u_*) only applies in cases of turbulence where longitudinal velocity is greater than 1 cm s^{-1} at 1 m above the sediment. Most of our velocities (obtained at 10 cm above the sediment) were within this

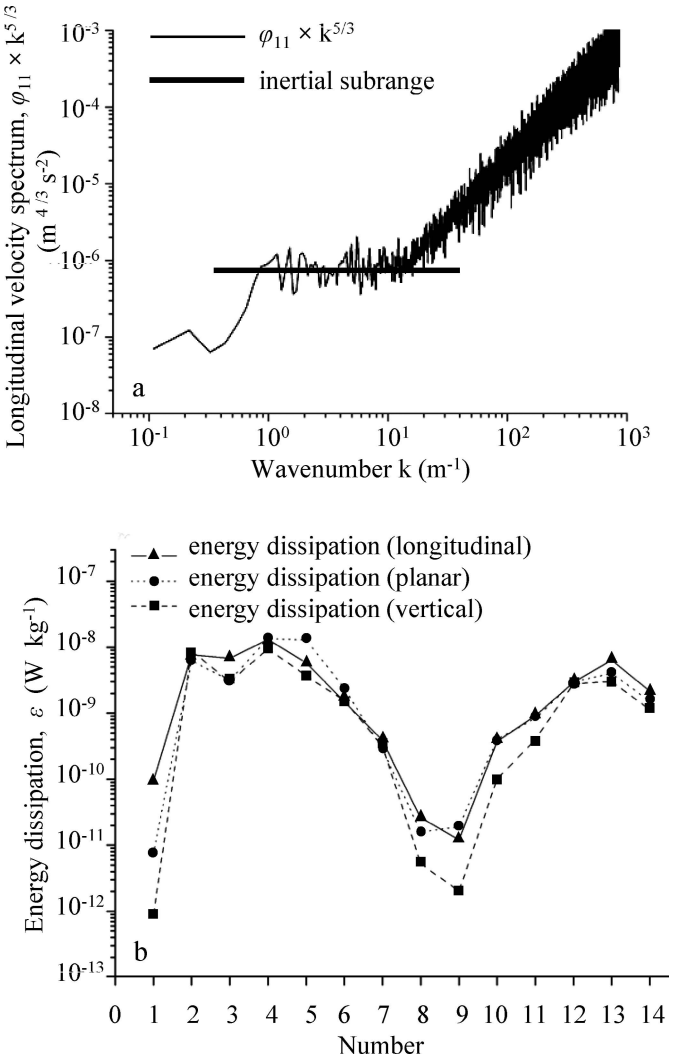

Fig. 2. (a) The measured longitudinal velocity spectrum φ_{11} (with $k^{-5/3}$ slope characteristic in the inertial subrange) is multiplied by $k^{5/3}$ to be independent of wave number k. The constant value of $\varphi_{11} \times k^{5/3}$, indicated by the horizontal bar, is used to calculate the mean energy dissipation (ε). (b) Dissipation rates (ε) calculated by inertial dissipation method using longitudinal, planar, and vertical velocity data as measured via acoustic Doppler velocimeter (ADV). Note similarity in longitudinal and transversal ε values.

range, with only velocities during the period of current reversal (profiles 7–9) falling significantly below this level (Fig. 3b). Accordingly, a majority of our profiles were consistent with the law-of-the-wall profile. However, for velocities smaller than this threshold, the logarithmic profile broke down and no characteristic features of the BBL could be identified (as independently confirmed by O_2 microsensor measurements). To verify the applicability of the law-of-the-wall to the full series of our velocity data, we employed the bottom drag coefficient (C_{1m}) via

$$u_* = \sqrt{C_{1m}}\, U_{1m}\left[\mathrm{m\ s^{-1}}\right] \tag{8}$$

where U_{1m} is the longitudinal velocity (m s^{-1}) at 1 m above the sediment obtained from the downward-looking ADP. The bottom drag coefficient relates the Reynolds stress on the sediment surface and the mean current velocity at a specified height. A C_{1m} value of 0.0033 was obtained for the full set of velocity data and a C_{1m} of 0.0013 was obtained when the velocity data below 1 cm s^{-1} were excluded. These C_{1m} values are comparable to the typical range of 0.001–0.003 (Wüest and Lorke 2003) for smooth-bottom boundaries (such as lake bottom sediments).

Temperature and O_2 distribution—Temperature and O_2 in the water column and near the sediment are shown to be strongly affected by seiche-induced variations in current velocity (Figs. 3, 4). At the beginning of the measurement period (21:00 h), a cold water mass from the central, well-mixed BBL moved across the experiment site (Fig. 4a–c). As the water mass shifted toward the northeast, warmer water from the upper BBL moved toward the experiment site (approaching 04:00 h) as the current reversal point was approached (Fig. 3). Following reversal of current direction, velocity increased and the cooler, well-mixed region of the BBL moved back to the experiment site as the current shifted the water mass toward the southwest.

Variations in temperature and O_2 in the BBL at 8 cm above the sediment are shown in Fig. 4a. Changes in temperature are shown as a function of depth in Fig. 4b (200 to 30 cm above the SWI) and Fig. 4c (1 cm above to 0.25 cm below the SWI). From Fig. 4b,c, it is apparent that while temperature varied over time (on the order of $\sim 2^{\circ}$C), the vertical temperature profile remained relatively constant with depth but was displaced first in the positive and then negative direction. However, while changes in O_2 are relatively minor (on the order of $\sim$ 10 μmol L^{-1}) at 8 cm above the sediment (Fig. 4a), O_2 variations are observed on a much greater scale near the SWI (Fig. 4d; 1 cm above to 0.25 cm below the SWI). When velocity decreased during profiles 5 to 9, O_2 decreased from $\sim$ 100 μmol L^{-1} to 70 μmol L^{-1} at 1 cm above the SWI and from 59 μmol L^{-1} to 5 μmol L^{-1} at the SWI. Furthermore, the sediment approached anoxia as sediment O_2 was depleted during this period.

The controlling influence that dynamic forcing has on the vertical distribution of O_2 above and below the SWI is emphasized in Fig. 5. O_2 profiles are separated into panels according to the direction of profile movement, which strongly corresponds to changes in velocity magnitude. The oscillating motion of the waterbody is apparent in the directional shifts of the O_2 profiles over the seiche cycle. As currents intensify, O_2 levels in the water and in the sediment increase, as shown by profiles 2–5 (Fig. 5a) and 9–14 (Fig. 5c); however, as velocity decreases approaching current reversal, O_2 throughout the full length of the profile drops to negligible levels (profiles 5–9; Fig. 5b). Profile 1 is not shown due to a slight misalignment with the other profiles that likely resulted from equipment settling into the sediment following deployment (discussed further below). A key point shown in Fig. 5 is the elasticity of the system, in that the vertical O_2 distribution changes significantly as it shifts from oxic (Fig. 5a) to nearly anoxic conditions (Fig. 5b), but then it returns to an oxic distribution (Fig. 5c) as it was in its initial state (Fig. 5a).

Table 2. Mean estimates of friction velocity (u_*), energy dissipation rate (ε), and intermittency ($\sigma_{\ln(\varepsilon)}$) of ε.

Profile number*	Time sensors contacted SWI*	Friction velocity, u_* (cm s^{-1})	Energy dissipation rate, ε (W kg^{-1})	ε intermittency, $\sigma_{\ln(\varepsilon)}$ (–)
1†	27 August 2007 21:14 h	(0.007)	(8.4×10^{-12})	(2.4)
2	22:05 h	0.067	7.5×10^{-9}	0.2
3	22:57 h	0.055	4.0×10^{-9}	0.5
4	23:50 h	0.079	1.2×10^{-8}	0.2
5	28 August 2007 00:42 h	0.064	6.5×10^{-9}	0.6
6	01:36 h	0.042	1.8×10^{-9}	0.3
7	02:27 h	0.024	3.2×10^{-10}	0.2
8	03:19 h	0.008	1.3×10^{-11}	0.8
9	04:12 h	0.007	7.8×10^{-12}	1.2
10	05:05 h	0.022	2.5×10^{-10}	0.8
11	05:59 h	0.030	6.7×10^{-10}	0.5
12	06:53 h	0.049	2.9×10^{-9}	0.0
13	07:44 h	0.056	4.2×10^{-9}	0.4
14	08:37 h	0.040	1.6×10^{-9}	0.3

* Data are compared by profile number, which represents the time each microsensor profile was obtained during the Alpnach campaign. The time assigned to each profile was the time at which the microsensor encountered the SWI.
† Outlier data for profile 1 placed in parentheses.

In Fig. 5a (profiles 2–5) and Fig. 5c (profiles 9–14), the oxic zone extends further into the sediment and δ_{DBL} decreases as velocity increases, clearly illustrating how current-induced mixing forces the vertical O_2 structure at the SWI. After velocity peaked at approximately 23:50 h (Fig. 5a), z_{max} and C_{SWI} reached maximum values (2.2 mm and 59 μmol L^{-1}, respectively), while δ_{DBL} reached a minimum of 1.0 mm. This relationship is shown in reverse in Fig. 5b (profiles 5–9) where, as velocity decreases during current reversal (between profiles 8 and 9 at approximately 04:00 h), δ_{DBL} increases to the point of being undefined, and the oxic zone almost completely disappears (minimum z_{max} = 0.3 mm) as the sediment goes anoxic.

O_2 flux and δ_{DBL}—Mean values of J_{O_2} and δ_{DBL} were obtained by averaging results from the five analytical methods used to evaluate O_2 profile and u_* data (Table 3). Consequently, both water-side (transport) and sediment-side (consumption) influences on J_{O_2} and δ_{DBL} are reflected in the average values. Values of J_{O_2} based on R_{O_2a} from the zonefit model were corrected for transient accumulation of O_2 per Eq. 2. During energetic periods (maximum $\varepsilon = 1.2 \times 10^{-8}$ W kg^{-1}; profile 4), δ_{DBL} reached a minimum of 1.0 mm and J_{O_2} increased to a maximum of 7.0 mmol m^{-2} d^{-1} (Table 3). As turbulence decreased approaching the current reversal point (minimum $\varepsilon = 7.8 \times 10^{-12}$ W kg^{-1}; profile 9), δ_{DBL} expanded significantly, since there was no longer sufficient turbulence to maintain an established DBL (Fig. 5; Table 3). Although a DBL in the classical sense is not maintained under these quiescent conditions (Gantzer and Stefan 2003; Røy et al. 2004), we nevertheless quantified δ_{DBL} during this period as a relative measure for comparison. Using independent results from all five methods, a maximum average δ_{DBL} of 7.8 ± 2.2 mm was estimated for profile 9 (Table 3).

During the period of weak turbulence and subsequently increased δ_{DBL}, J_{O_2} decreased by 85%, from 7.0 mmol m^{-2} d^{-1} to 1.1 mmol m^{-2} d^{-1} (Fig. 6). The substantial short-term variability in J_{O_2} in response to changes in turbulence is emphasized in Fig. 6. However, an explicit relationship between J_{O_2} and ε cannot be defined by the linear correlation shown in Fig. 6, since J_{O_2} is also affected by other variables (e.g., C_{bulk} and R_{O_2}).

The relatively small standard deviation of J_{O_2} and δ_{DBL} obtained from the different methods per profile as compared to the overall temporal variation in averages (J_{O_2} or δ_{DBL}) shows that similar estimates were obtained from the different methods (Table 3). Water-side methods did tend to yield somewhat higher values of J_{O_2} (with correspondingly lower values of δ_{DBL}). A comparative evaluation of method results is being performed for the companion methods study (L. Bryant, unpubl. data). Standard deviation evolves according to changes in turbulence. When turbulence levels are low, increasing δ_{DBL} and decreasing ε lead to greater uncertainty and subsequently higher σ (or intermittency) for these parameters. Thus, observed increases in variability in δ_{DBL} and ε during the period of weak turbulence (Tables 2 and 3) are more an effect of analysis than a reflection of the quality of data. While J_{O_2}, δ_{DBL}, and ε values for profile 1 exhibit unusually high variability, these increased deviations are reflected in data obtained with multiple instruments (ADV and microprofiler; Tables 2 and 3) and are observed only at the beginning of the campaign; hence, they are likely a result of equipment settling at the lake bottom following deployment.

Sediment oxic zone—Changes in the extent of the sediment oxic zone correspond to variations in J_{O_2} and δ_{DBL} in response to turbulence. When O_2 transport into the sediment escalated as the DBL was compressed by elevated turbulence (Fig. 6), both z_{max} (Fig. 5) and the vertically integrated mass of O_2 (M_{O_2}; Table 4) increased significantly as O_2 penetrated deeper into the sediment. The oxic zone is observed to reach a maximum z_{max} of 2.2 mm during active turbulence (corresponding δ_{DBL} = 1.0 mm, J_{O_2} = 6.9 mmol m^{-2} d^{-1}, and M_{O_2} = 54 μmol m^{-2}). Conversely, z_{max} decreased to a minimum of 0.3 mm and C_{SWI}

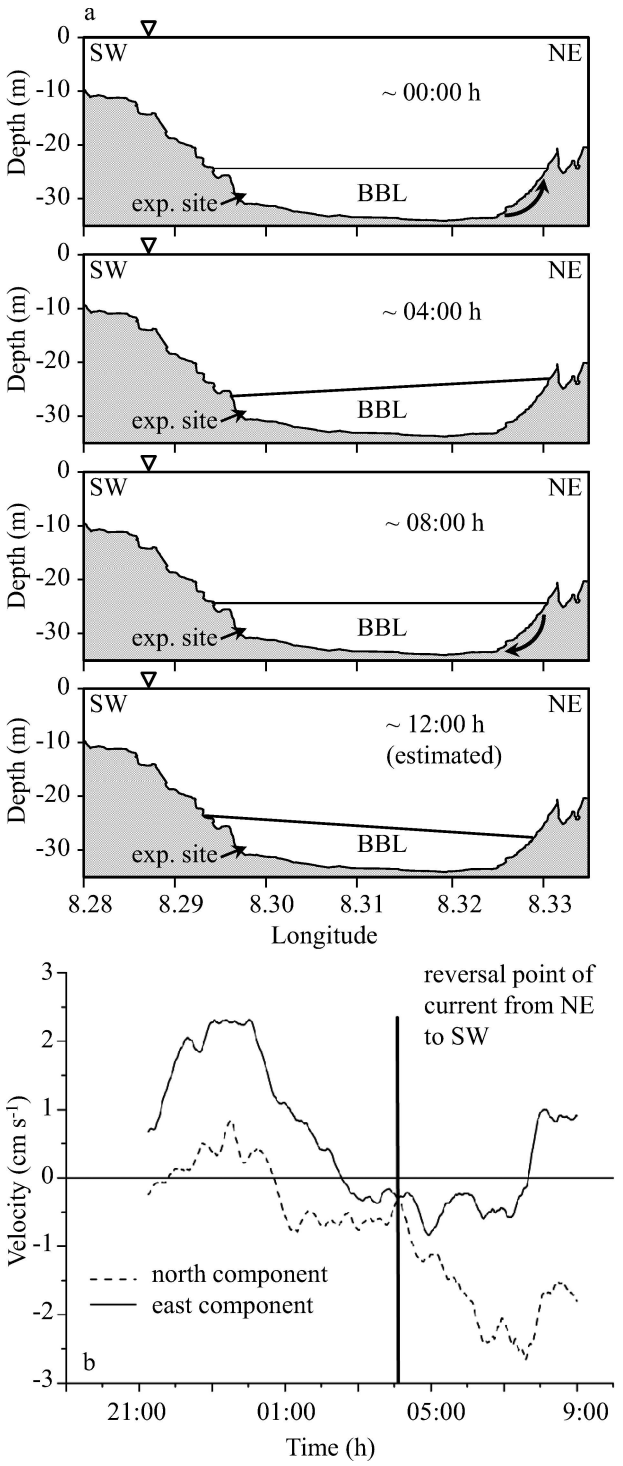

Fig. 3. (a) Seiche cycle in Lake Alpnach and location of experiment site during 27–28 August 2007 campaign. Note that water surface is indicated by downward-facing triangles and that scale of seiche is approximate. (b) East and north velocity components at 10 cm above the sediment as measured by the ADV. Bold vertical line marks the current reversal point where seiche-induced motion of the waterbody changed direction from northeast (NE) to southwest (SW).

decreased from 59 to 5 μmol L^{-1} during negligible turbulence (corresponding δ_{DBL} = 7.6 mm, J_{O_2} = 1.3 mmol m^{-2} d^{-1}, and M_{O_2} = 3 μmol m^{-2}) as the sediment approached anoxia. The strongly coupled behavior observed in these parameters is supported by recent modeling work based on data from Lake Alpnach (Brand et al. 2009), which shows that an increase in δ_{DBL} (from 0.25 to 1.5 mm) results in decreased z_{max} (from 1.7 to 1.2 mm) and decreased J_{O_2} (from 15 to 9.5 mmol m^{-2} d^{-1}).

Profile dynamics—Eq. 2 was used to determine proximity to steady state. Although significant variation was observed in our O_2 profiles over the 12-h measurement period (Fig. 5), O_2 accumulation and/or depletion within the sediment was insignificant (Table 4), with an average $\partial C/\partial t_a$ of $\pm$0.30 mmol m^{-2} d^{-1}, or $\sim$ 5% of the average J_{O_2} (5.2 mmol m^{-2} d^{-1}) over the full measurement period. The rate at which O_2 enters the sediment (J_{O_2}) equals the areal O_2 consumption rate (R_{O_2a}) at steady state (Eq. 2), and these values were found to be almost equivalent in our mesotrophic lake system (Table 4). Additionally, the average J_{O_2} and M_{O_2} (32 μmol m^{-2}; Table 4) for the 12-h period indicate a mean O_2 residence time in the sediment of 9 min. Because profiles were obtained every $\sim$ 50 min, quasi–steady-state conditions prevailed.

Discussion

Forcing of O_2 *distribution*—Lorke et al. (2003) show that δ_{DBL} is controlled primarily by turbulence rather than velocity based on an observed phase lag between ε, δ_{DBL}, and current velocity, where ε and δ_{DBL} lagged consistently ($\sim$ 1.5 h) behind current velocity at 1 m above the sediment. Although we do observe a direct relationship between ε and δ_{DBL}, a defined phase lag between these parameters and current velocity was not evident within the temporal resolution of our measurements (Fig. 7). However, it has been shown that this delay becomes greater with increasing distance from the sediment (Lorke et al. 2002). The phase lag would therefore be expected to be much shorter ($\sim$ 10 min) during our experiment.

During periods of relatively high velocity (profiles 1–5 and 9–14), turbulence increased as cold water from the deeper region of the BBL moved across our experiment site (Figs. 4, 7). The movement of this cooler water mass along the slope may have established small inverse temperature gradients that produced additional turbulence due to bottom convective mixing (Lorke et al. 2005). Turbulence compressed the DBL during these periods, which facilitated increased O_2 transport from the BBL down to the sediment and resulted in greater sediment O_2 uptake and an enhanced sediment oxic zone. As the water mass approached current reversal (profiles 5–9), decreased turbulence, J_{O_2}, and z_{max} are observed as current velocity subsided (Figs. 5, 6).

Temperatures in the BBL and near the SWI increased (Fig. 4a–c) in response to the influx of warm water from farther up the slope (confirmed by CTD data, not shown). Variations in temperature are reflected over the full microsensor profile depth and are not affected by changes

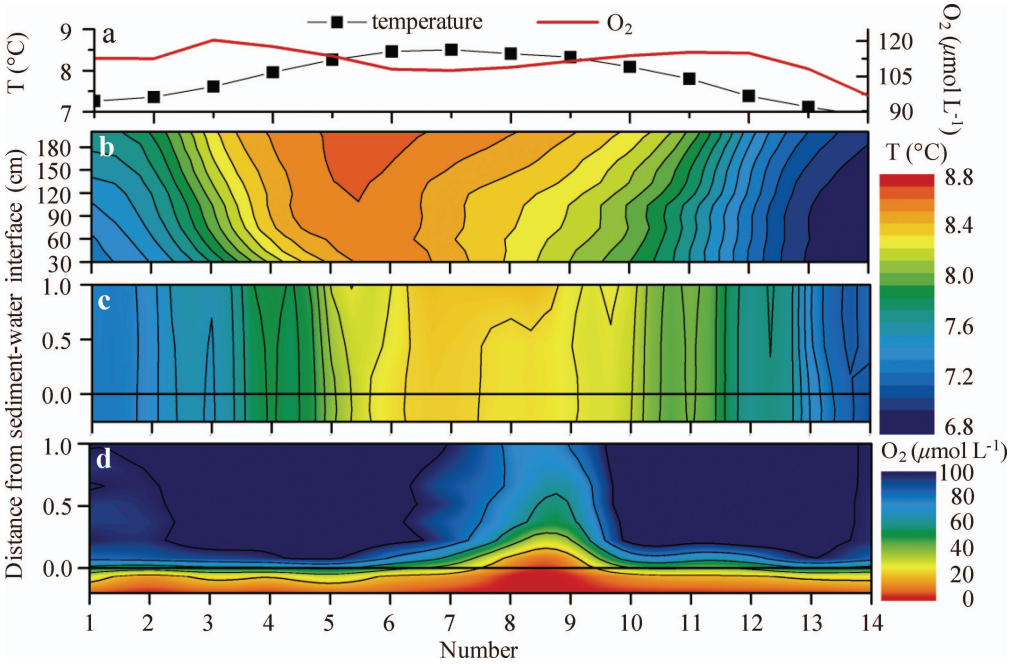

Fig. 4. Temperature and O_2 data obtained on 27–28 August 2007. (a) Temperature (T) and O_2 time series as measured using a T-O_2 logger at 8 cm above sediment. (b) Temperature contour plot showing data from 30 cm to 200 cm above sediment as measured via thermistors. (c and d) Temperature and O_2 contour plots showing data from −0.25 cm (in sediment) up to 1 cm (in water) as measured via microprofiler microsensors (14 profiles throughout 12-h measurement period).

in δ_{DBL}, which is likely due to the relatively rapid rate of heat transfer (compared to molecular diffusion) and the fact that temperature is not consumed by the sediment (unlike O_2). Hence, once the near-surface sediment temperature equilibrates with that of the BBL, the sediment no longer behaves as a heat sink. Conversely, significant variation was observed in the vertical distribution of O_2 across the SWI, which may be largely attributed to O_2 consumption. In the absence of turbulence, while O_2 remained at ~ 110 μmol L^{-1} several centimeters above the SWI, the O_2 supply through the extended DBL was insufficient to maintain the sediment oxic zone (Figs. 4, 6). As J_{O_2} diminished and O_2 was consumed in the sediment, O_2 in the water immediately overlying the sediment, C_{SWI}, and z_{max} decreased significantly (Figs. 4, 5). These findings emphasize that, even when O_2 levels in the BBL remain relatively high, the O_2 distribution on both sides of the SWI and the corresponding J_{O_2} are strongly governed by turbulence, as supported by previous work (Jørgensen and Revsbech 1985; Brand et al. 2009; Gantzer et al. 2009*a*).

Variations in sediment O_2 *consumption*—Quasi-steady-state conditions prevailed (J_{O_2} and R_{O_2a} differed by only 5%) and, correspondingly, both J_{O_2} and R_{O_2} (quantified by R_{O_2a} and R_{O_2v}) varied in response to dynamic forcing, as shown by R_{O_2a} data in Table 4. This indicates that sediment O_2 consumption was directly related to O_2 availability within the sediment as supplied via J_{O_2}. Monod and first-order kinetic models are used to characterize sediment O_2 consumption as a function of O_2 concentration in the sediment (Rasmussen and Jørgensen 1992; Higashino et al. 2004). However, due to the variety of O_2-consuming processes and the complexity of the kinetics, simple zero-order kinetics is frequently assumed (Bouldin 1968; Jørgensen and Boudreau 2001; Røy et al. 2004). Irrespective of the kinetics, though, it has been reported that when O_2 uptake is at least partially governed by diffusive transport, R_{O_2} does become dependent on O_2 concentration below O_2 levels of 20–30 μmol L^{-1} (Santschi et al. 1990; Berg et al. 2003). Sediment O_2 levels remained close to this minimum range during our study (Fig. 5). Our results therefore demonstrate dependence of R_{O_2} on O_2 availability under limiting O_2 conditions regardless of the kinetics involved. Models based on variable zones of O_2 consumption and Monod kinetics were used (zonefit and model methods, respectively) to evaluate J_{O_2} and δ_{DBL} with comparable results (Table 3; L. Bryant unpubl. data).

Variability in sediment O_2 consumption was further evaluated using PROFILE (zonefit method) to characterize regions of differing R_{O_2v} within the sediment oxic zone as a function of time and depth, as shown in Fig. 8. Zone-specific R_{O_2v} values predicted by PROFILE were corrected for $\partial C/\partial t_v$ (Eq. 2). PROFILE results show that R_{O_2v} was consistently higher near the SWI and then decreased significantly with depth (Fig. 8). Results by O'Connor and Harvey (2008) and Brand et al. (2009) also show increased R_{O_2v} immediately below the SWI. O_2 consumption in the upper sediment region is often elevated as a result of mineralization of freshly deposited organic matter at the sediment surface as well as reoxidation of subsequently released reduced inorganic species (Santschi et al. 1990; Zhang et al. 1999). Accordingly, increased heterotrophic bacterial abundance and activity in the sediment surface layer is common (Fischer et al. 2002, 2005).

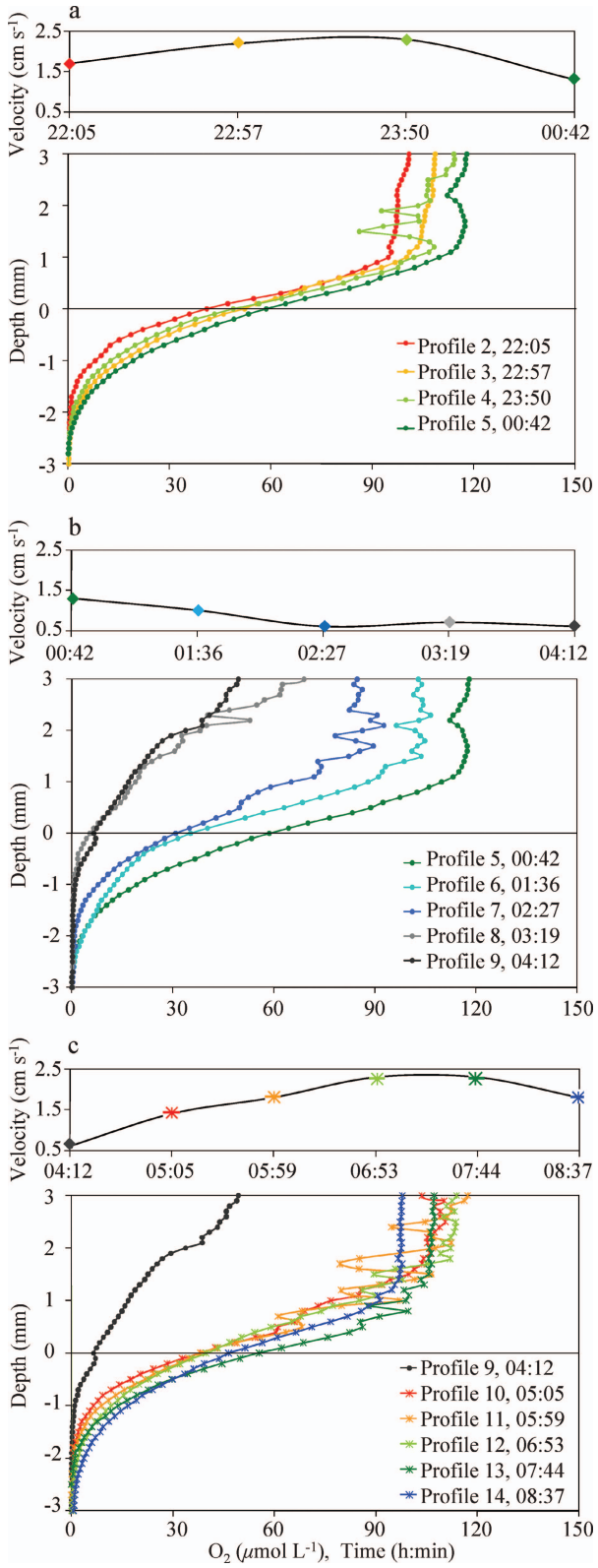

Fig. 5. O_2 microprofiles obtained at approximately 50-min intervals relative to the ADV velocity time series. O_2 profiles are divided into three panels with corresponding section of velocity time series plotted above each O_2 profile panel (a–c). (a) Initially, current velocity is increasing and the O_2 profiles are observed to shift to the right toward more oxic conditions in both the water and the sediment with a corresponding decrease in δ_{DBL} and increase in z_{max}. (b) As velocity decreases, δ_{DBL} is shown to increase and z_{max} to decrease as the profiles shift to the left toward anoxic conditions in the sediment and overlying water. (c) As velocities return to initial levels, the O_2 profiles are observed to shift back to the right toward a more oxic distribution similar to that observed in (a).

Variations in turbulence (Fig. 8a) coupled with changes in PROFILE-predicted consumption zones (Fig. 8b–d) support our observation of increased J_{O_2} leading to increased O_2 consumption (Table 4). The upper sediment layer is obviously most directly affected by turbulence in the BBL and variations in δ_{DBL}. Consumption in this upper zone is observed to increase during periods of peak turbulence when elevated O_2 concentrations above the sediment and a thinner δ_{DBL} facilitate enhanced J_{O_2}. Elevated R_{O_2v} in the upper sediment as a result of increased O_2 availability implies that the intrinsic capacity of the sediment for O_2 consumption (PSOD) exceeds J_{O_2}, indicating water-side control of sediment O_2 uptake (O'Connor and Harvey 2008). When J_{O_2} increased in response to elevated turbulence, the sediment oxic zone is observed to increase while $\partial C/\partial t_a$ remained relatively small; this supports that the additional O_2 entering the sediment was being consumed rather than accumulating in the sediment (Fig. 8b,d; Table 4). During the period when turbulence is at a minimum and δ_{DBL} extends to the point of becoming undefined, thereby limiting O_2 transport and subsequent availability at the SWI, consumption is characterized by a minimal zone and R_{O_2v} drops significantly (Fig. 8c). At this point, the sediment oxic zone almost completely disappears. The elasticity observed in sediment–water O_2 profiles shown in Fig. 5 is also evident in sediment O_2 consumption zones shown in Fig. 8, although it is less direct because of the complexity of sediment processes. The distribution of O_2 consumption zones for profile 13 (Fig. 8d) returns to a structure similar to that of profile 4 (Fig. 8b) when turbulence increases after a substantial shift to a smaller, single zone for profile 8 during the stagnant period (Fig. 8c).

Our results show that variations in δ_{DBL} have a significant effect on J_{O_2}, R_{O_2} (both areally and volumetrically), and resultant z_{max}. It is important to emphasize that in this study, diffusion time for O_2 across the DBL and transport time through the sediment oxic zone are comparable ($\sim$ 10 to 20 min during the majority of the campaign when turbulence levels were high enough to maintain a defined DBL). When the timescale of O_2 diffusion through the DBL is short in comparison to transport through the sediment oxic zone (e.g., oligotrophic environments where z_{max} can be measured in centimeters and sediment O_2 residence time can be on the order of days), changes in δ_{DBL} would be unlikely to have a strong influence on J_{O_2}, R_{O_2}, and z_{max} (Glud et al. 2007).

Scale of variation—Mean values for J_{O_2} (Table 4) obtained during this study are comparable to values found

Table 3. Results of the five analytical methods used for sediment O_2 uptake rate (J_{O_2}) and diffusive boundary layer thickness (δ_{DBL}) calculations.

Method	Profile number	1	2	3	4	5	6	7	8	9	10	11	12	13	14
Direct: measured gradient	δ_{DBL} (mm)	0.6	0.9	1.3	1.0	1.0	1.4	1.9	5.9	6.3	1.4	1.3	2.2	0.8	1.0
	J_{O_2} (mmol m^{-2} d^{-1})	9.9	8.1	5.1	7.6	7.0	6.5	4.5	1.6	1.2	6.8	7.2	4.0	7.6	5.5
u_*: function of friction velocity	δ_{DBL} (mm)	3.0	0.8	0.9	0.8	0.8	1.2	1.9	4.6	6.7	1.6	1.2	1.5	0.7	0.9
	J_{O_2} (mmol m^{-2} d^{-1})	2.0	9.0	7.6	9.6	8.2	7.8	4.6	2.0	1.2	5.8	8.0	5.7	8.1	6.4
Curvefit: best fit of single curve	δ_{DBL} (mm)	1.3	1.3	1.2	1.3	1.1	2.2	2.2	8.7	11.1	1.6	2.0	1.9	0.9	1.2
	J_{O_2} (mmol m^{-2} d^{-1})	4.5	6.0	5.6	5.9	6.1	4.1	3.9	1.1	0.7	5.9	4.7	4.5	6.8	4.6
Zonefit: fitting multiple zones via PROFILE	δ_{DBL} (mm)	1.2	1.1	1.3	1.2	1.1	1.7	2.4	9.3	6.0	1.6	1.7	2.1	0.9	1.3
	J_{O_2} (mmol m^{-2} d^{-1})	5.2	7.1	5.4	6.4	6.1	5.3	3.5	1.0	1.3	5.8	5.6	4.0	6.9	4.4
Model: DBL estimation via AQUASIM	δ_{DBL} (mm)	1.0	1.8	1.2	1.5	0.9	1.7	2.2	9.7	9.0	2.2	2.0	1.7	1.0	0.9
	J_{O_2} (mmol m^{-2} d^{-1})	5.9	4.3	5.7	5.4	7.3	5.2	3.9	1.0	0.9	4.3	4.7	5.1	5.9	6.4
Average of five methods	δ_{DBL} (mm)	1.4±0.9	1.2±0.4	1.2±0.2	1.2±0.3	1.0±0.1	1.6±0.4	2.1±0.2	7.6±2.3	7.8±2.2	1.7±0.3	1.6±0.4	1.9±0.3	0.9±0.1	1.1±0.2
	J_{O_2} (mmol m^{-2} d^{-1})	5.5±2.9	6.9±1.8	5.9±1.0	7.0±1.7	6.9±0.9	5.8±1.4	4.1±0.5	1.3±0.5	1.1±0.3	5.7±0.9	6.1±1.5	4.7±0.7	7.0±0.8	5.5±0.9

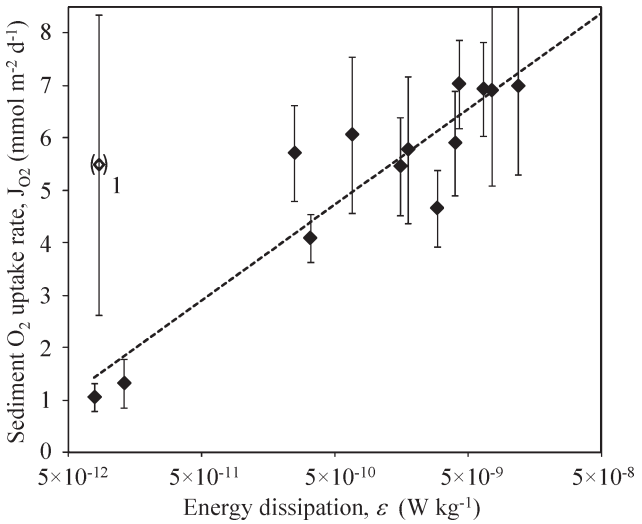

Fig. 6. Correlation between ε and sediment O_2 uptake rate (J_{O_2}). The linear trendline serves as a guide for the reader's eye and does not imply an explicit relationship between J_{O_2} and ε. Because data for profile 1 are outliers, as discussed in the text, these data are placed in parentheses.

in previous studies of BBL turbulence at the same location. Brand et al. (2008) estimated an average J_{O_2} of 13 ± 2 mmol m^{-2} d^{-1} and Lorke et al. (2003) estimated J_{O_2} to range from 6 to 13 mmol m^{-2} d^{-1}, with a corresponding δ_{DBL} range of 0.16 to 0.84 mm. Turbulence and O_2 levels in the BBL were higher in these previous studies than those observed during our campaign; this is reflected in our relatively low turbulence estimates and subsequently decreased J_{O_2} and increased δ_{DBL} values. Despite the less energetic conditions, variation in J_{O_2} and the vertical

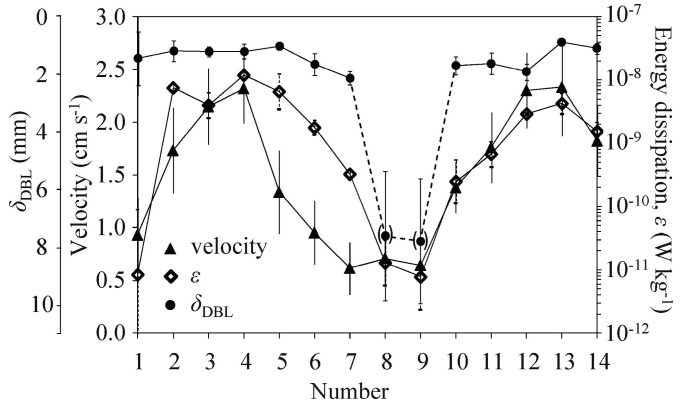

Fig. 7. Time series of current velocity, turbulence (as defined by ε), and δ_{DBL} showing close correlation between all three parameters with only a slight phase lag (on the order of minutes) between velocity and ε. Similarity in δ_{DBL} estimates obtained from different analytical methods is indicated by low standard deviations for δ_{DBL}. The DBL becomes undefined during the period of negligible turbulence and thus corresponding δ_{DBL} data (profiles 8 and 9) are placed in parentheses with dashed-line connectors to emphasize that these data are included solely as a relative comparison. Note reversed axis for δ_{DBL}.

Table 4. Average J_{O_2} and vertically integrated areal rates of change in the O_2 concentration over time ($\partial C/\partial t_a$), areal sediment O_2 consumption rates (R_{O_2a}), and mass of O_2 (M_{O_2}) in the sediment.

Profile number	J_{O_2} (mmol m^{-2} d^{-1})	$\partial C/\partial t_a$*† (mmol m^{-2} d^{-1})	R_{O_2a}* (mmol m^{-2} d^{-1})	M_{O_2}* (μmol m^{-2})
1	5.5	−0.68	6.2	50
2	6.9	−0.11	7.0	26
3	5.9	0.14	5.8	42
4	7.0	0.16	6.8	36
5	6.9	−0.02	7.0	54
6	5.8	−0.42	6.2	34
7	4.1	−0.44	4.5	23
8	1.3	−0.25	1.6	3
9	1.1	0.28	0.8	5
10	5.7	0.31	5.4	24
11	6.1	0.11	6.0	28
12	4.7	0.16	4.5	32
13	7.0	0.17	6.9	40
14	5.5	0.11	5.3	44
Average	5.2	±0.30	5.3	32

* Profile-specific areal values of R_{O_2a}, $\partial C/\partial t_a$, and M_{O_2} represent the integral over the depth of the sediment oxic zone. $\partial C/\partial t_a$ was evaluated for each profile as follows: the profiles immediately before and after were compared (e.g., profiles 2 and 4 were compared to evaluate profile 3) to calculate the areal rate of change in O_2 ($\partial C/\partial t_a$).

† Quasi–steady state is established by relatively insignificant values of $\partial C/\partial t_a$ (5% of average J_{O_2}).

distribution of O_2 over the 12-h measurement period was still significant (Figs. 5–7). The fact that we observed such change in these parameters in response to dynamic, though relatively mild, turbulence conditions highlights the dependence of sediment O_2 uptake on turbulence.

Not only was J_{O_2} found to vary significantly over the duration of a single seiche cycle (on the order of hours) during our campaign (Fig. 6), but it was also observed to change substantially on a subhourly timescale. For example, in the course of the 53-min period between profiles 9 and 10 when turbulence increased as the waterbody shifted back toward the southwest direction following current reversal, J_{O_2} increased from 1.1 mmol m^{-2} d^{-1} to 5.7 mmol m^{-2} d^{-1} (Table 4). During this time, ε increased from 7.8×10^{-12} to 2.5×10^{-10} W kg^{-1}, δ_{DBL} decreased from 7.8 to 1.7 mm (Fig. 7), z_{max} increased from 0.6 to 1.3 mm (Fig. 5), and M_{O_2} increased from 5 to 24 μmol m^{-2} (Table 4). The high degree of variation observed in J_{O_2} and the vertical O_2 distribution over such a brief time period illustrates the transient nature of sediment O_2 uptake. While it has been shown that long-term (e.g., annual) average J_{O_2} is typically not influenced by short-term (e.g., hourly) changes in δ_{DBL} (Glud et al. 2007), our results stress the importance of taking turbulence into account when resolving O_2 profiles in order to fully evaluate J_{O_2}. Under dynamic conditions, a system must be characterized in greater detail than what can be discerned from a single profile. An accurate assessment of J_{O_2} and R_{O_2} is not possible without obtaining a comprehensive series of profiles describing the full range of variation in the vertical distribution of O_2. Furthermore, extreme caution should be taken in evaluating PSOD based on R_{O_2v} analyses without considering physical limitations on O_2 transport to the SWI (and subsequent O_2 availability in the sediment) and proximity to long-term steady state. Variation in PROFILE-predicted R_{O_2v} results for individual profiles (Fig. 8) emphasizes how evaluating R_{O_2v} based on a single profile could lead to very different estimates of PSOD. In all likelihood, the average R_{O_2v} observed during our 12-h campaign (3.5 mmol m^{-3} d^{-1} in upper sediment; data not shown) may still significantly underestimate actual PSOD due to the mild turbulence conditions limiting sediment O_2 availability and subsequent consumption.

Technical and logistical restraints often limit the number of in situ microsensor measurements obtained during a given deployment to only a few (Glud et al. 2009), which may be an issue depending on the timescale of the dynamics in the system of interest. During this study, we were able to obtain 14 microprofiles at approximately 50-min intervals. Fluctuations in δ_{DBL} have been previously observed at timescales on the order of seconds (Røy et al. 2004; O'Connor and Hondzo 2008). However, Brand et al. (2009) show that the influence of these rapid variations in δ_{DBL} is negligible on evaluations of mean J_{O_2} and the vertical O_2 distribution near the SWI at timescales appropriate for defining seiche cycles (e.g., minutes, hours). The subhourly timescale at which we assessed data is small compared to the 8-h duration of the seiche cycle; thus, a thorough characterization of how seiche-induced variations in sediment O_2 uptake was achieved.

In conclusion, our results reveal the effect of natural dynamic forcing on the vertical distribution of O_2 across the SWI and on sediment O_2 uptake. Although work has been done that contributes significantly to the understanding of BBL dynamics and flux pathways, these studies have been largely laboratory or model based (Røy et al. 2004; Glud et al. 2007; O'Connor and Hondzo 2008). Previous in situ studies have focused primarily on physical, water-side controls of O_2 transport (Gundersen and Jørgensen 1990; Lorke et al. 2003) or spatial and temporal variations in O_2 distribution in sediment (Epping and Helder 1997; Glud et al. 2003, 2009). This study is novel in that we analyzed O_2 uptake from both sides of the SWI. In doing so, we have

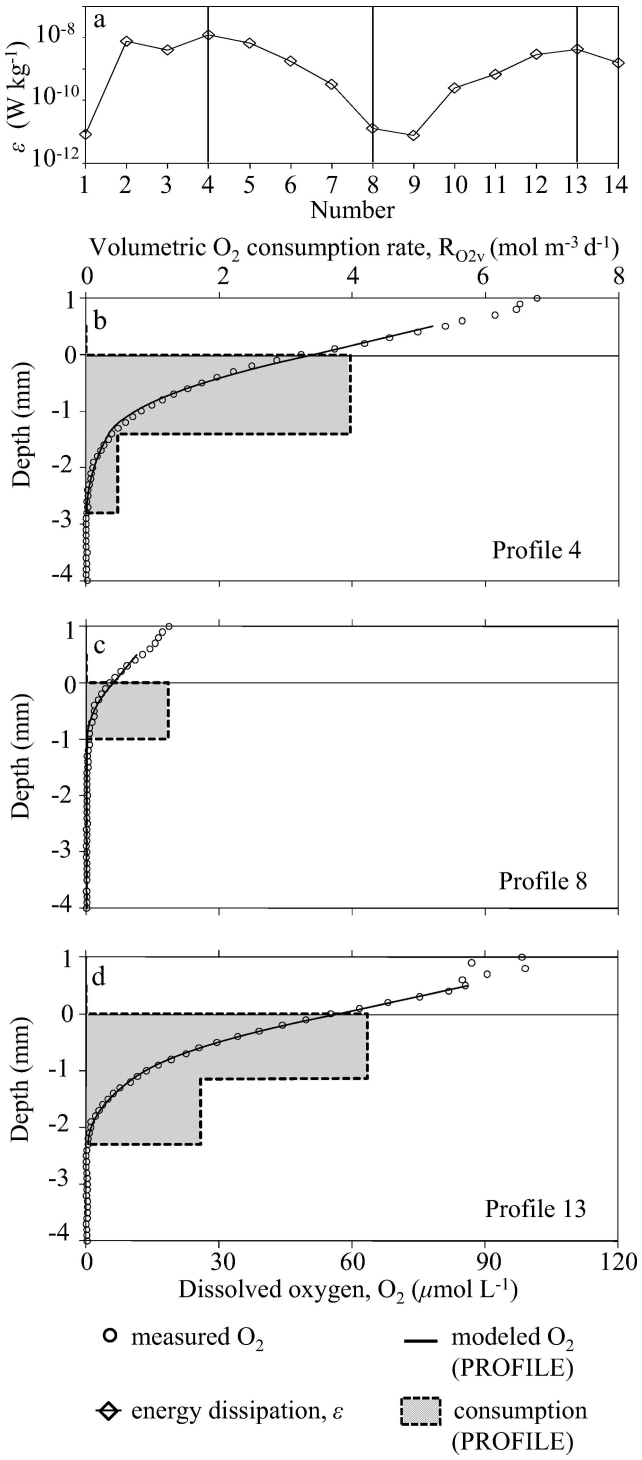

Fig. 8. PROFILE model results defining zones of varying volumetric sediment O_2 consumption rates (R_{O_2v}) for periods of active and inactive turbulence as characterized by ε in (a). During elevated turbulence (b and d), O_2 consumption is characterized by two zones. However, a single zone defines low consumption during the period of negligible turbulence (c).

expanded on previous results by analyzing the tight coupling between water-side (turbulence, as characterized by ε) and sediment-side (O_2 consumption in sediment, as characterized by R_{O_2}) processes influencing sediment O_2 uptake under actual field conditions in a freshwater system. The highly transient nature of J_{O_2} is revealed by rapid changes in the vertical distribution of O_2 in both the water and the sediment in response to dynamic forcing via seiche motion. R_{O_2} was shown to adjust quickly to variations in J_{O_2} at quasi–steady state. Although our study focused on O_2 fluxes, knowledge gained regarding the relationship between turbulence and mass transfer at the SWI can be more broadly applied to fluxes of other soluble chemical species (e.g., reduced metals, hydrogen sulfide, methane) as well (Jørgensen et al. 1979; Frenzel et al. 1990; Gantzer et al. 2009*b*). The crucial role of turbulence is highlighted by the fact that, despite relatively high O_2 levels only a few centimeters above the sediment, O_2 transport to the SWI and the extent of the sediment oxic zone both decreased substantially during quiescent periods. The critical control that dynamic forcing can have on J_{O_2} must be considered when evaluating sediment O_2 uptake via measuring devices (e.g., benthic chambers) that do not capture natural turbulence conditions. Furthermore, based on the significant changes observed in J_{O_2} during periods as brief as an hour, our results show that using isolated J_{O_2} measurements may be insufficient, particularly in systems experiencing high levels of variable turbulence.

Acknowledgments

We are grateful to Peter Berg and Miki Hondzo for their useful advice. We also thank Lorenzo Rovelli, Michi Schurter, Christian Dinkel, and Mathias Kirf, who offered invaluable assistance in the field and with equipment. Helpful feedback from Ronnie Glud, Hans Røy, and an anonymous reviewer substantially improved the manuscript. The research described in this paper has been funded in part by the U.S. Environmental Protection Agency (EPA) under the Science to Achieve Results (STAR) Graduate Fellowship Program. The EPA has not officially endorsed this publication, and the views expressed herein may not reflect the views of the EPA. This research was also supported by the U.S. National Science Foundation (NSF) through the Integrative Graduate Education and Research Traineeship (IGERT) program (DGE 0504196) and by the Swiss National Science Foundation, grants 200020-111763 and 200020-120128.

References

Arega, F., and J. H. W. Lee. 2005. Diffusional mass transfer at sediment-water interface of cylindrical sediment oxygen demand chamber. J. Environ. Eng.-ASCE **131:** 755–766, doi:10.1061/(ASCE)0733-9372(2005)131:5(755)

Baker, M. A., and C. H. Gibson. 1987. Sampling turbulence in the stratified ocean: Statistical consequences of strong intermittency. J. Phys. Oceanogr. **17:** 1817–1836, doi:10.1175/1520-0485(1987)017<1817:STITSO>2.0.CO;2

Berg, P., N. Risgaard-Petersen, and S. Rysgaard. 1998. Interpretation of measured concentration profiles in sediment pore water. Limnol. Oceanogr. **43:** 1500–1510.

———, S. Rysgaard, and B. Thamdrup. 2003. Dynamic modeling of early diagenesis and nutrient cycling. A case study in an arctic marine sediment. Am. J. Sci. **303:** 905–955, doi:10.2475/ajs.303.10.905

Beutel, M. W. 2003. Hypolimnetic anoxia and sediment oxygen demand in California drinking water reservoirs. Lake Reserv. Manage. **19:** 208–221, doi:10.1080/07438140309354086

Boudreau, B. P. 2001. Solute transport above the sediment-water interface, p. 104–126. *In* B. P. Boudreau and B. B. Jørgensen [eds.], The benthic boundary layer: Transport processes and biogeochemistry. Oxford Univ. Press.

Bouldin, D. R. 1968. Models for describing the diffusion of oxygen and other mobile constituents across the mud-water interface. J. Ecol. **56:** 77–87, doi:10.2307/2258068

Brand, A., C. Dinkel, and B. Wehrli. 2009. Influence of the diffusive boundary layer on the solute dynamics in the sediments of a seiche-driven lake: A model study. J. Geophys. Res. **114**, G01010, doi:10.1029/2008JG000755

———, D. F. McGinnis, B. Wehrli, and A. Wüest. 2008. Intermittent oxygen flux from the interior into the bottom boundary of lakes as observed by eddy correlation. Limnol. Oceanogr. **53:** 1997–2006.

———, and others. 2007. Microsensor for in situ flow measurements in benthic boundary layers at submillimeter resolution with extremely slow flow. Limnol. Oceanogr. Methods **5:** 185–191.

Dalsgaard, T. and others [eds.]. 2000. Protocol handbook for NICE—Nitrogen Cycling in Estuaries: A project under the EU research programme: Marine Science and Technology (MAST III). National Environmental Research Institute, Silkeborg, Denmark, http://www2.dmu.dk/LakeandEstuarineEcology/nice/NICE_handbook.pdf.

Epping, E. H. G., and W. Helder. 1997. Oxygen budgets calculated from in situ microprofiles for Northern Adriatic sediments. Cont. Shelf Res. **17:** 1737–1764, doi:10.1016/S0278-4343(97)00039-3

Fischer, H., F. Kloep, S. Wilzcek, and M. T. Pusch. 2005. A river's liver—microbial processes within the hyporheic zone of a large lowland river. Biogeochemistry **76:** 349–371, doi:10.1007/s10533-005-6896-y

———, S. C. Wanner, and M. Pusch. 2002. Bacterial abundance and production in river sediments as related to the biochemical composition of particulate organic matter (POM). Biogeochemistry **61:** 37–55, doi:10.1023/A:1020298907014

Frenzel, P., B. Thebrath, and R. Conrad. 1990. Oxidation of methane in the oxic surface layer of a deep lake sediment (Lake Constance). FEMS Microbiol. Ecol. **73:** 149–158, doi:10.1111/j.1574-6968.1990.tb03935.x

Gantzer, C. J., and H. G. Stefan. 2003. A model of microbial activity in lake sediments in response to periodic water-column mixing. Water Res. **37:** 2833–2846, doi:10.1016/S0043-1354(03)00110-6

Gantzer, P. A., L. D. Bryant, and J. C. Little. 2009*a*. Effect of hypolimnetic oxygenation on oxygen depletion rates in two water-supply reservoirs. Water Res. **43:** 1700–1710, doi:10.1016/j.watres.2008.12.053

———, ———, and ———. 2009*b*. Controlling soluble iron and manganese in a water-supply reservoir using hypolimnetic oxygenation. Water Res. **43:** 1285–1294, doi:10.1016/j.watres.2008.12.019

Glud, R. N. 2008. Oxygen dynamics of marine sediments. Mar. Biol. Res. **4:** 243–289, doi:10.1080/17451000801888726

———, P. Berg, H. Fossing, and B. B. Jørgensen. 2007. Effect of the diffusive boundary layer on benthic mineralization and O_2 distribution: A theoretical model analysis. Limnol. Oceanogr. **52:** 547–557.

———, J. K. Gundersen, N. P. Revsbech, and B. B. Jørgensen. 1994. Effects on the benthic diffusive boundary layer imposed by microelectrodes. Limnol. Oceanogr. **39:** 462–467.

———, ———, H. Røy, and B. B. Jørgensen. 2003. Seasonal dynamics of benthic O_2 uptake in a semi enclosed bay: Importance of diffusion and fauna activity. Limnol. Oceanogr. **48:** 1265–1276.

———, H. Stahl, P. Berg, F. Wenzhöfer, K. Oguri, and H. Kitazato. 2009. In situ microscale variation in distribution and consumption of O_2: A case study from a deep ocean margin sediment (Sagami Bay, Japan). Limnol. Oceanogr. **54:** 1–12.

Grant, H. L., R. W. Stewart, and A. Moilliet. 1962. Turbulence spectra from a tidal channel. J. Fluid Mech. **12:** 241–268, doi:10.1017/S002211206200018X

Gundersen, J. K., and B. B. Jørgensen. 1990. Microstructure of diffusive boundary layers and the oxygen uptake of the sea floor. Nature **345:** 604–607, doi:10.1038/345604a0

Higashino, M., C. J. Gantzer, and H. G. Stefan. 2004. Unsteady diffusional mass transfer at the sediment/water interface: Theory and significance for SOD measurement. Water Res. **38:** 1–12, doi:10.1016/j.watres.2003.08.030

———, B. L. O'Connor, M. Hondzo, and H. G. Stefan. 2008. Oxygen transfer from flowing water to microbes in an organic sediment bed. Hydrobiologia **614:** 219–231, doi:10.1007/s10750-008-9508-8

———, and H. G. Stefan. 2005. Sedimentary microbial oxygen demand for laminar flow over a sediment bed of finite length. Water Res. **39:** 3153–3166, doi:10.1016/j.watres.2005.05.032

Hondzo, M., T. Feyaerts, R. Donovan, and B. L. O'Connor. 2005. Universal scaling of dissolved oxygen distribution at the sediment–water interface: A power law. Limnol. Oceanogr. **50:** 1667–1676.

Jørgensen, B. B., and B. P. Boudreau. 2001. Diagenesis and sediment-water exchange, p. 211–244. *In* B. P. Boudreau and B. B. Jørgensen [eds.], The benthic boundary layer: Transport processes and biogeochemistry. Oxford Univ. Press.

———, and N. P. Revsbech. 1985. Diffusive boundary layers and the oxygen uptake of sediments and detritus. Limnol. Oceanogr. **30:** 111–122.

———, ———, T. H. Blackburn, and Y. Cohen. 1979. Diurnal cycle of oxygen and sulfide microgradients and microbial photosynthesis in a cyanobacterial mat sediment. Appl. Environ. Microbiol. **38:** 46–58.

Li, Y.-H., and S. Gregory. 1974. Diffusion of ions in sea water and in deep-sea sediments. Geochim. Cosmochim. Acta **38:** 703–714, doi:10.1016/0016-7037(74)90145-8

Lorke, A., B. Müller, M. Maerki, and A. Wüest. 2003. Breathing sediments: The control of diffusive transport across the sediment–water interface by periodic boundary-layer turbulence. Limnol. Oceanogr. **48:** 2077–2085.

———, F. Peeters, and A. Wüest. 2005. Shear-induced convective mixing in bottom boundary layers on slopes. Limnol. Oceanogr. **50:** 1612–1619.

———, L. Umlauf, T. Jonas, and A. Wüest. 2002. Dynamics of turbulence in low-speed oscillating bottom-boundary layers of stratified basins. Environ. Fluid Mech. **2:** 291–313, doi:10.1023/A:1020450729821

Mackenthun, A. A., and H. G. Stefan. 1998. Effect of flow velocity on sediment oxygen demand: Experiments. J. Environ. Eng.-ASCE **124:** 222–230, doi:10.1061/(ASCE)0733-9372(1998)124:3(222)

Müller, B., M. Maerki, C. Dinkel, R. Stierli, and B. Wehrli. 2002. In situ measurements in lake sediments using ion-selective electrodes with a profiling lander system, p. 126–143. *In* M. Taillefert and T. F. Rozan [eds.], Environmental electrochemistry: Analyses of trace element biogeochemistry. ACS symposium series 811, American Chemical Society.

Münnich, M., A. Wüest, and D. M. Imboden. 1992. Observations of the second vertical mode of the internal seiche in an alpine lake. Limnol. Oceanogr. **37:** 1705–1719.

O'Connor, B. L., and J. W. Harvey. 2008. Scaling hyporheic exchange and its influence on biogeochemical reactions in aquatic ecosystems. Water Resour. Res. **44:** W12423, doi:10.1029/2008WR007160

———, and M. Hondzo. 2008. Dissolved oxygen transfer to sediments by sweep and eject motions in aquatic environments. Limnol. Oceanogr. **53:** 566–578.

Rasmussen, H., and B. B. Jørgensen. 1992. Microelectrode studies of seasonal oxygen uptake in a coastal sediment: Role of molecular diffusion. Mar. Ecol. Prog. Ser. **81:** 289–303, doi:10.3354/meps081289

Reichert, P. 1994. AQUASIM—a tool for simulation and data analysis of aquatic systems. Water Sci. Technol. **30:** 21–30.

Røy, H., M. Huettel, and B. B. Jørgensen. 2004. Transmission of oxygen concentration fluctuations through the diffusive boundary layer overlying aquatic sediments. Limnol. Oceanogr. **49:** 686–692.

Santschi, P., P. Höhener, G. Benoit, and M. Buchholtz-Ten brink. 1990. Chemical processes at the sediment-water interface. Mar. Chem. **30:** 269–315, doi:10.1016/0304-4203(90)90076-O

Stachowitsch, M., B. Riedel, M. Zuschin, and R. Machan. 2007. Oxygen depletion and benthic mortalities: The first in situ experimental approach to documenting an elusive phenomenon. Limnol. Oceanogr. Methods **5:** 344–352.

Veenstra, J. N., and S. L. Nolen. 1991. In situ sediment oxygen demand in five southwestern U.S. lakes. Water Res. **25:** 351–354, doi:10.1016/0043-1354(91)90016-J

Wetzel, R. G. 2001. Limnology: Lake and river ecosystems, 3rd ed. Academic.

Wüest, A., and A. Lorke. 2003. Small-scale hydrodynamics in lakes. Annu. Rev. Fluid Mech. **35:** 373–412, doi:10.1146/annurev.fluid.35.101101.161220

———, G. Piepke, and D. C. Van Senden. 2000. Turbulent kinetic energy balance as a tool for estimating vertical diffusivity in wind-forced stratified waters. Limnol. Oceanogr. **45:** 1388–1400.

Wyngaard, J. C., and O. R. Coté. 1971. The budgets of turbulent kinetic energy and temperature variance in the atmospheric surface layer. J. Atmos. Sci. **28:** 190–201, doi:10.1175/1520-0469(1971)028<0190:TBOTKE>2.0.CO;2

Zhang, H., W. Davison, and C. Ottley. 1999. Remobilisation of major ions in freshly deposited lacustrine sediment at overturn. Aquat. Sci. **61:** 354–361, doi:10.1007/s000270050071

Associate editor: Ronnie Nøhr Glud

Received: 25 March 2009
Accepted: 26 October 2009
Amended: 10 December 2009